Generating Lithium-Ion Cell Thermodynamic Efficiency Maps

Felix-A Lebel, Joao Pedro Trovao, Loic Boulon, Ali Sari, Serge Pelissier, Pascal Venet

▶ **To cite this version:**

Felix-A Lebel, Joao Pedro Trovao, Loic Boulon, Ali Sari, Serge Pelissier, et al.. Generating Lithium-Ion Cell Thermodynamic Efficiency Maps. VPPC, Aug 2018, Chicago, IL, United States. hal-02013904v1

HAL Id: hal-02013904

https://hal.science/hal-02013904v1

Submitted on 11 Feb 2019 (v1), last revised 14 Apr 2021 (v2)

HAL is a multi-disciplinary open access archive for the deposit and dissemination of scientific research documents, whether they are published or not. The documents may come from teaching and research institutions in France or abroad, or from public or private research centers.

L'archive ouverte pluridisciplinaire **HAL**, est destinée au dépôt et à la diffusion de documents scientifiques de niveau recherche, publiés ou non, émanant des établissements d'enseignement et de recherche français ou étrangers, des laboratoires publics ou privés.

Generating Lithium-Ion Cell Thermodynamic Efficiency Maps

Félix-A. LeBel[1], João Pedro Trovão[1], Loïc Boulon[2], Ali Sari[3], Serge Pelissier[4], and Pascal Venet[3]

[1]Univ. de Sherbrooke, Centre des Technologies Avancées (CTA-BRP-UdeS), Sherbrooke, Qc, J1K 2R1, Canada
[2]Univ. du Québec Trois-Rivières (UQTR), Trois-Rivières, Qc, G9A 5H7, Canada
[3]Univ. Lyon, Univ. Claude Bernard Lyon 1, Centrale Lyon, INSA Lyon, CNRS, Ampère, 69000 Villeurbanne, France
[4]Université de Lyon, IFSTTAR, AME, LTE, 69500 Bron, France

***Abstract*—In lithium-ion cells, heat is generated via joules losses and exothermic electro-chemical reactions, causing cells to self-heat and risk premature aging or catastrophic failure. However, heat generation is not constant throughout the cells discharge, due to the complex chemical reactions and changes in the micro structure of the active materials of the electrodes. Non-linear or complex systems thermodynamic behavior is commonly represented by efficiency maps, generated from empirical data. These empirical models are used to estimate a system heat generation at a given operating state. Although very common in many fields of engineering, efficiency maps are yet to be used for lithium-ion batteries. This paper presents a simple method to achieve accurate estimation of thermodynamic efficiency over the full range of use. In this method, the thermodynamic losses are assumed to be proportional to the measured ohmic resistance of the cell. This empirical method is intended to be a fast and reliable characterization tool that can replace other modeling methods, while capturing the non-linear nature of lithium-ion cells. It can be used for energy management and assessment purposes, for battery design or for thermal management system sizing and control.**

INTRODUCTION

Nowadays, electric vehicles (EVs) represent an increasing market share of vehicles sold world wide. Battery powered EVs are seen as the most suited technology to reduce green house gas emissions in transportation, alongside fuelcells [1]. The overall energy efficiency of the powertrain of an EV is about 80%, meanwhile combustion engines have an efficiency ranging from 10% to 34% at best [2], [3]. This goes without considering the wasted energy and resources necessary to transformation and distribution of gasoline [4]. Despite being mostly produced from fossil fuels today, electricity production from renewable sources is for-casted to increase, to nearly satisfy the global energy demand by 2050 [5].

Thermodynamic efficiency , η, is the ratio of the useful energy of a system to the total energy [6]. Knowing the thermodynamic efficiency of a system is useful to estimate its losses. It can be used for energy management or performance estimation purposes [4], [7] . In the case of lithium-ion batteries (LiBs), the stored energy gets mostly converted into heat and electricity. Some of the chemical reactions will release or absorb heat because of variations of the entropy of the materials [8]. However these are not considered as losses, as they are reversible mechanisms.

The efficiency of certain simple systems can sometimes be assumed constant. Although it may be true for an operation point, thermodynamic efficiency of lithium-ion cells is not constant throughout its entire usage domain. Electrical properties of the cell are dependent of the reactions kinetics, temperature and state of charge (SOC). Indeed, the heat generation of LiBs is highly dependent on its SOC and current [9]. Efficiency over the entire operation domain of a complex or non-linear system can be represented in the form of two dimensional contour maps, known as efficiency maps. Electric motors [10] or combustion engines [11] performances are often mapped this way. Efficiency maps are good system level empirical models that can be used by engineers to solve various problems, such as optimization problems [12], [13] or component sizing [14]. Few paper present an efficiency map for LiBs discharge [13]. This paper provides a methodology to experimentally obtain them, as it seems to be missing from the literature.

The paper is structured as follows: Firstly, the experimental setup is presented at section I. Then, the proposed characterization method is exposed at section II. Section III presents a validation of the results, comparing computed values to measurements. Finally, conclusions are drawn at section **??**.

I. EXPERIMENTAL SETUP

The lithium-ion cells tested used for this work have a Nickel manganese cobalt (NMC) positive electrode and graphite negative electrode. They are commercially available cylindrical 18650 cells of a measured capacity $Q_{cell,nom}$ of 2.90Ah. Their operational voltage ranges from 2.5V at a Depth of Discharge (DOD) of 100% to 4.2V at $DOD = 0\%$. Commercially available cell holders with an intrinsic resistance of 20mΩ are used to hold the cells in place on the custom made circuit board, shown in Fig. 1. The positive and negative poles of the cell were connected to the output and sense terminals of programmable source/load, using the 4 wire method. The experiment was performed with an Arbin BT-2000.

The cell was placed in a climatic chamber at a temperature setpoint of 20°C, for the entire duration of the experiment.

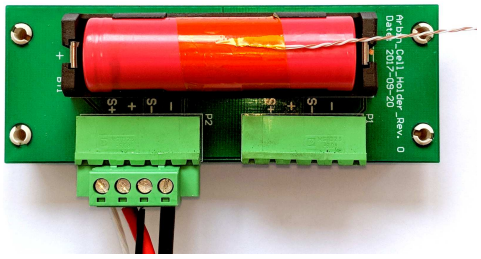

Fig. 1. Experimental setup

II. Cell characterization

Full domain characterization is obtained by sweeping the entire allowable C-rate range, with currents of 250mA, 500mA, 1A and up to 13A, by increments of 0.65A, as shown in Fig. 2. Negative currents indicate discharge and positive currents recharge of the cell.

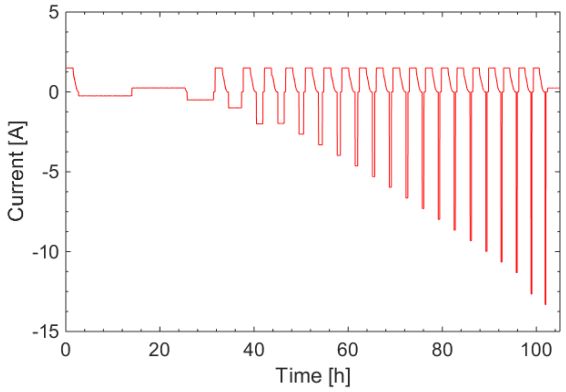

Fig. 2. Current profile

Lower voltage limit was set at 2.5V during constant current discharge, as can be seen in Fig. 3. Each discharge was followed by a rest period of 30 minutes, to allow for cell temperature to cool down to ambient temperature T_{amb} of 20°C. A constant current (CC) recharge of 1.5A with an upper voltage limit of 4.2V (Fig. 3) then followed each discharge, with a constant voltage (CV) top off at a minimum current of 50mA, as recommended by the cell manufacturer. Again, recharge was followed by a 30 minutes rest time to allow for the cell to stabilize to T_{amb} and voltage to relax.

A. Discharge potential

Fig. 4 shows the discharge voltage of the cell. From these, one can extract specifications such as capacity and internal resistance R_{cell}. The dotted line on Fig. 4 is the pseudo open circuit voltage (pseudo-OCV) V_0 and is defined by 1, as the average between a low current charge (+250mA) and symmetric discharge (-250mA), assuming that the average of both voltages approximates to the open-circuit voltage of the cell at a given SOC or DOD. Hysteresis effects are also being neglected.

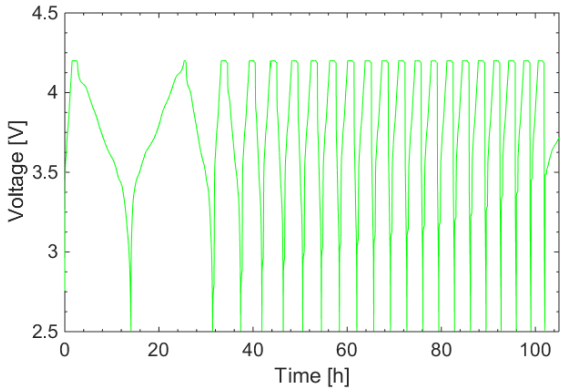

Fig. 3. Voltage response

$$V_0(DOD) = \frac{V_+(DOD, +250mA) + V_-(DOD, -250mA)}{2} \quad (1)$$

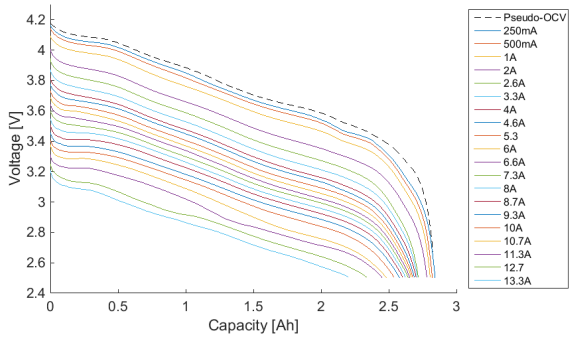

Fig. 4. Cell pseudo-OCV (dashed) and terminal voltage (plain) for discharges of 250mA to 13.3A, by 0.65A increments

B. Internal resistance

The internal resistance R_{cell} is the result of electrical conduction and ionic migration phenomenas. These include: resistivity of the current collector, resistivity of the active materials, ion transport in the electrolyte, among others. Ionic conductivity in the electrolyte depends of cell's temperature and reaction kinetics, i.e. the current flowing in the cell, leading to different ionic concentration gradient in the electrolyte [15], [16]. However, $R_{cell}(DOD, I)$ can be computed by a discretized Ohm's law, where dV is the drop of circuit voltage $V(DOD, I)$ caused by current at a given DOD, from pseudo-OCV $V_0(DOD, I)$ (2). Fig. 5 shows $R_{cell}(DOD, I)$ in the form of a 3D mesh plot as a function of current and DOD, computed from the discharges presented at Fig. 4. The measured average internal resistance over the whole domain is 74mΩ. Internal resistance decreases as current increases, possibly because of the higher internal temperature, causing improvements in ionic migration in the electrolyte and improving the electrochemical reaction in general. Achieving

iso-thermal conditions at high discharge rates can be quite challenging. Hence, this implies that this map is dependent on cooling conditions of the cell.

$$R_{cell}(DOD, I) = \left| \frac{V_0(DOD) - V(DOD, I)}{I} \right| \quad (2)$$

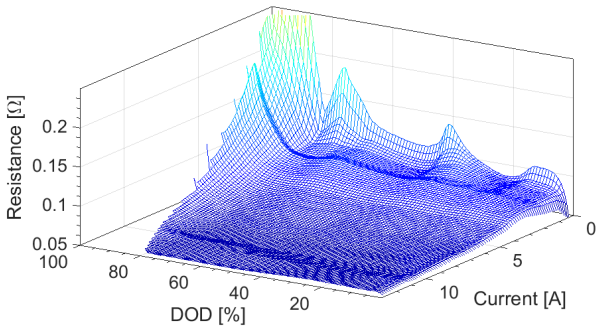

Fig. 5. Internal resistance map,

C. Electrical power

Two informations are necessary to compute the cells thermodynamic efficiency: electrical power and losses. One can estimate the useful power $P_{max}(DOD, I)$ with the maximum power transfer theorem (3), which is the maximum of (6) quadratic equation. Fig. 6 show the iso-power map of the cell as a function of DOD and current. One can see that in order for a cell to provide a steady power, the current has to increase an amount proportional to its drop in potential and corresponding internal resistance.

$$P_{max}(DOD, I) = \frac{V_0^2(DOD)}{4R_{cell}(DOD, I)} \quad (3)$$

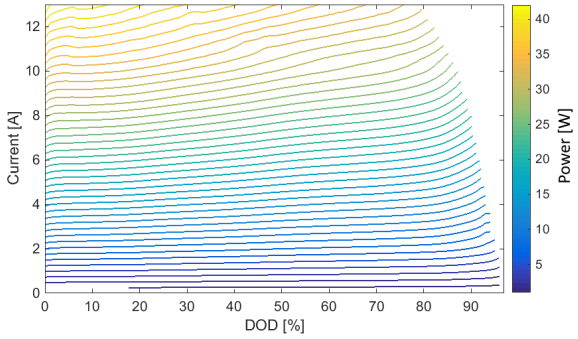

Fig. 6. Iso power [W] as a function of current and DOD

D. Losses

Although entropy changes cause both heating or cooling of the cell, it is assumed in this work that heat losses are purely exothermic and caused by the internal resistance (or impedance) of the cell. While this may affect cell temperature, this hypothesis remains valid from a thermodynamic standpoint. Heat generation from the flow of electrons and ions in the cell can be computed by (4).

$$\dot{Q}(DOD, I) = R_{cell}(DOD, I)I^2 \quad (4)$$

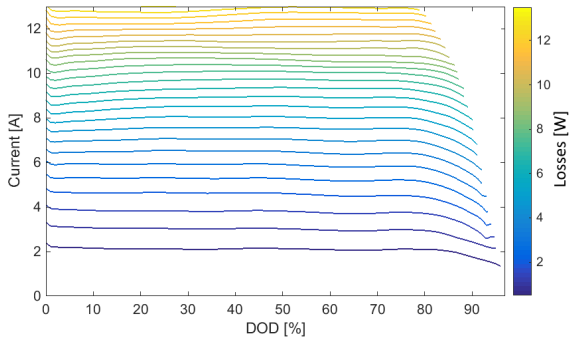

Fig. 7. Heat losses [W] function of current and DOD

E. Efficiency map computation

Thermodynamic efficiency $\eta_{cell}(DOD, I)$ during discharge of a cell (Fig. 8) is the ratio of $P_{max}(DOD, I)$ to the total power, given as the sum of $P_{max}(DOD, I)$ and $\dot{Q}(DOD, I)$, from a thermodynamical standpoint (5).

$$\eta_{cell}(DOD, I) = \frac{P_{max}(DOD, I)}{P_{max}(DOD, I) + \dot{Q}(DOD, I)} \quad (5)$$

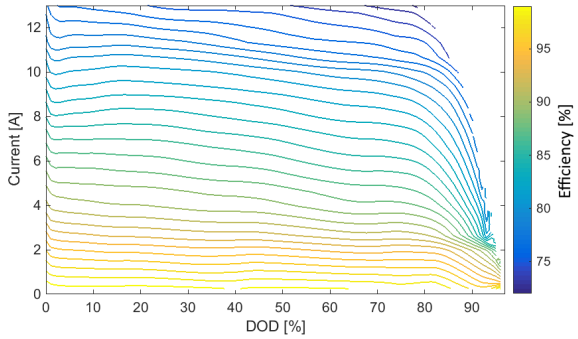

Fig. 8. Efficiency [%] function of current and DOD

III. Validation

The useful power of the battery was measured during the characterization cycling schedule. This measured power was compared to the estimated power given by (6), by using the current measurements I_{meas} and the calculated pseudo-OCV V_0 and R_{cell}.

$$P_{cell}(DOD, I) = V_0(DOD)I - R_{cell}(DOD, I)I^2 \quad (6)$$

Fig. 9 shows a very good match between the measured (plain) and calculated (dashed) discharge powers P_{cell} for all tested currents.

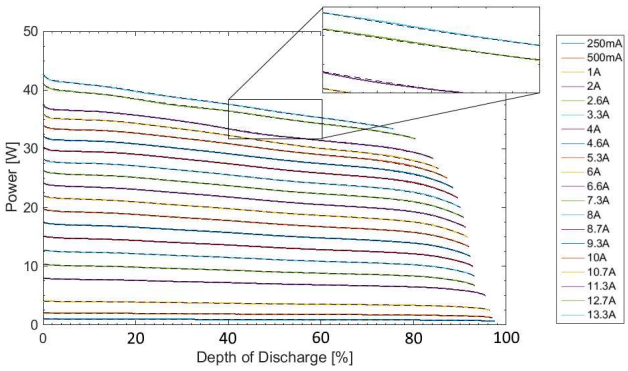

Fig. 9. Measured electric power (plain), estimated power (dashed) of the cell during discharge at various currents

One can observe an error of less than 1% between the measure power and estimated power from the internal resistance, thus validating the method. The error is mainly caused by numerical interpolation and measurement noise. In order to validate the heat losses calculated from the internal resistance map, a temperature model could be implemented. The temperature from the model could then be compared to the measured temperature. However, this is intended for future works.

IV. Conclusion

The methodology provided in this paper can help develop research and engineering of lithium-ion batteries, by building empirical maps. Although the efficiency map obtained show a good match in terms of predicting output power, further work would be required to validate the heat losses. This would require to develop a thermal model of the cell for instance, which is planed for future works. However, transitory behavior due to the electrochemical kinetics are not considered in these maps. They should be considered for near steady-state purposes, as it may overestimate the internal impedance of a cell. For short current impulses, cell efficiency is likely to be better than what has been determined with the presented method, because the relaxation periods between pulses allow for lithium-ion concentration in the electrolyte to increase, thus making species more available during discharges. The empirical maps are good for cells of similar chemistry and same level of degradation. Efficiency maps are intended for system level engineering. For instance, they can be used to size a battery pack of an EV for a given operation point. Another application of these would be for power sharing strategies in hybrid vehicles, maximizing the overall fuel efficiency. A third possible usage of these maps could be to determine the operating temperature of a cell and use it to estimate the aging rate of a pack. Internal resistance and efficiency maps could also help in material research, studying the effect of discharge rate on chemical reaction kinetics. Similar methodology could apply to any electric energy storage devices, such as supercapacitors, lithium-ion capacitors, lead-acid batteries.

Acknowledgment

This work was supported in part by Allcell Technologies, Canada Research Chairs Program, Natural Sciences and Engineering Research Council of Canada, and also developed with the support from "*Service de Coopération et d'Action Culturelle du Consulat Général de France à Québec*" under the Samuel De Champlain program.

References

[1] G. van de Kaa, D. Scholten, J. Rezaei, and C. Milchram, "The battle between battery and fuel cell powered electric vehicles: A bwm approach," *Energies*, vol. 10, no. 11, 2017.

[2] H. Laitinen, A. Lajunen, and K. Tammi, "Improving electric vehicle energy efficiency with two-speed gearbox," in *2017 IEEE Vehicle Power and Propulsion Conference (VPPC)*, pp. 1–5, Dec 2017.

[3] K. K. Prabhakar, M. Ramesh, A. Dalal, C. U. Reddy, A. K. Singh, and P. Kumar, "Efficiency investigation for electric vehicle powertrain with variable dc-link bus voltage," in *IECON 2016 - 42nd Annual Conference of the IEEE Industrial Electronics Society*, pp. 1796–1801, Oct 2016.

[4] J. P. T. ao and P. G. Pereirinha, "Multiple energy sources hybridization: The future of electric vehicles?," in *New Generation of Electric Vehicles* (Z. Stevic, ed.), ch. 8, Rijeka: InTech, 2012.

[5] S. Teske, J. Muth, S. Sawyer, T. Pregger, S. Simon, T. Naegler, M. O'Sullivan, S. Schmid, J. Pagenkopf, B. Frieske, W. Graus, K. Kermeli, W. Zittel, J. Rutovitz, S. Harris, T. Ackermann, R. Ruwahata, and N. Martense, "Energy [r] evolution-a sustainable world energy outlook," *Greenpeace International, EREC and GWEC*, 2012.

[6] R. Heldson, "Chapter one - energy," in *Introduction to Applied Thermodynamics* (R. Heldson, ed.), The Commonwealth and International Library: Mechanical Engineering Division, pp. 1 – 11, Pergamon, 1965.

[7] J. Trovao, M. A. Roux, E. Menard, and M. R. Dubois, "Energy- and power-split management of dual energy storage system for a three-wheel electric vehicle," *IEEE Transactions on Vehicular Technology*, vol. 66, pp. 5540–5550, July 2017.

[8] K. Takano, Y. Saito, K. Kanari, K. Nozaki, K. Kato, A. Negishi, and T. Kato, "Entropy change in lithium ion cells on charge and discharge," *Journal of Applied Electrochemistry*, vol. 32, pp. 251–258, Mar 2002.

[9] "Sae j1312: Procedure for mapping engine performance-spark ignition and compression ignition engines," 1980.

[10] R. Bojoi, E. Armando, M. Pastorelli, and K. Lang, "Efficiency and loss mapping of ac motors using advanced testing tools," in *2016 XXII International Conference on Electrical Machines (ICEM)*, pp. 1043–1049, Sept 2016.

[11] V. Celik and E. Arcaklioglu, "Performance maps of a diesel engine," vol. 81, pp. 247–259, 07 2005.

[12] K. Gökce and A. Ozdemir, "An instantaneous optimization strategy based on efficiency maps for internal combustion engine/battery hybrid vehicles," *Energy Conversion and Management*, vol. 81, pp. 255 – 269, 2014.

[13] A. Demircal, P. Sergeant, S. Koroglu, S. Kesler, E. ztrk, and M. Tumbek, "Influence of the temperature on energy management in battery-ultracapacitor electric vehicles," *Journal of Cleaner Production*, vol. 176, pp. 716 – 725, 2018.

[14] E. Grunditz, *BEV Powertrain Component Sizing with Respect to Performance, Energy Consumption and Driving Patterns*. Department of Energy and Environment, Chalmers University of Technology, 2014.

[15] A. Lievre, A. Sari, P. Venet, A. Hijazi, M. Ouattara-Brigaudet, and S. Pelissier, "Practical online estimation of lithium-ion battery apparent series resistance for mild hybrid vehicles," *IEEE Transactions on Vehicular Technology*, vol. 65, pp. 4505–4511, June 2016.

[16] A. Tron, A. Nosenko, Y. D. Park, and J. Mun, "Enhanced ionic conductivity of the solid electrolyte for lithium-ion batteries," *Journal of Solid State Chemistry*, vol. 258, pp. 467 – 470, 2018.